

Broad-Band Antireflection Coating at Near-Infrared Wavelengths by a Breath Figure

Min Soo Park and Jin Kon Kim*

National Creative Research Initiative Center for Block Copolymer Self-Assembly, Department of Chemical Engineering and Polymer Research Institute, Electric and Computer Engineering Division, Pohang University of Science and Technology, Kyungbuk 790-784, Korea

Received May 12, 2005. In Final Form: August 18, 2005

We prepared a porous thin film by spin-coating of a cellulose acetate butyrate (CAB) solution in tetrahydrofuran under a humid environment. Due to evaporative cooling during spin-coating, condensed water droplets were formed by a breath figure on the CAB solution, and these developed a porous structure after complete drying. By varying the solution concentration and rotating speeds, two distinct morphologies were generated: top and bottom layers with higher and lower porosities, respectively. We found that the two-layer porous film coated on glass exhibited low reflectance of less than 1% in the near-infrared (NIR) regime corresponding to wavelengths between 900 and 2200 nm. Since the porous structure was very uniform over a large area, the film could be easily employed for broad-band antireflection coating at NIR wavelengths.

1. Introduction

Breath figure formation, which has long been a fascinating phenomenon in nature, has become a simple and useful technique for the preparation of porous polymer films.^{1–13} It utilizes solvent-evaporative cooling on the surface of a solution under humid conditions on which water vapors are condensed into water droplets at the solution surface. Then, water droplets interact with one another and are finally hexagonally packed. After complete evaporation of the solvent and water, traces of water droplets remain in the polymer film and become pores with a honeycomb structure. The pore sizes formed by the breath figure range from a few hundreds of nanometers to several micrometers depending on the amount of water inlet by humidity (or the humid air flow rate), evaporation speed, and polymer concentration.

Porous polymer films prepared by a breath figure have been used for the assembly of nanoparticles^{14–17} and templates to transfer the structures to metallic and other

organic materials for photonic crystals¹⁸ and microlens arrays.¹⁹ A superhydrophobic surface was generated by peeling off the upper layer of the ordered porous film.²⁰ Also, holes for containing picoliters were produced.²¹ All of these applications based on the breath figure utilize the “drop and evaporation” method, in which a polymer solution is dropped onto a glass substrate and evaporated under humid air flow or a humid environment.

Recently, we introduced a new method to prepare a breath figure by “spin-coating of a polymer solution under a humid environment”.¹² This method allowed the formation of a uniform porous polymer film over a large area (several square centimeters). In this study, we extended this method to broad-band antireflection (AR) coating in the near-infrared (NIR) regime corresponding to wavelengths between 900 and 2200 nm. AR coating in the NIR region has been used in transmitting optics, for instance, output couplers, dichroic mirrors, lenses, and windows, to eliminate light reflection from an AR-coated surface where the signals or energy of light is received.^{22,23} The principle of AR coating is based on the destructive interference of reflected light from interfaces between the air and a film, one film and another film in the case of a multilayered film coating, and a film and a substrate.²⁴ The two-layer design among many AR coatings uses a quarter wavelength thickness of an individual layer:²⁴

* To whom correspondence should be addressed. Fax: +82-54-279-8298. E-mail: jkkim@postech.ac.kr.

(1) Widawski, G.; Rawiso, M.; François, B. *Nature* **1994**, *369*, 387–389.

(2) François, B.; Pitois, O.; François, J. *Adv. Mater.* **1995**, *7*, 1041–1044.

(3) Pitois, O.; François, B. *Eur. Phys. J. B* **1999**, *8*, 225–231.

(4) Pitois, O.; François, B. *Colloid Polym. Sci.* **1999**, *277*, 574–578.

(5) Srinivasarao, M.; Collings, D.; Philips, A.; Patel, S. *Science* **2001**, *292*, 79–83.

(6) Song, L.; Bly, R. K.; Wilson, J. N.; Bakbak, S.; Park, J. O.; Srinivasarao, M.; Bunz, U. H. F. *Adv. Mater.* **2004**, *16*, 115–118.

(7) Limaye, A. V.; Narhe, R. D.; Dhote, A. M.; Ogale, S. B. *Phys. Rev. Lett.* **1996**, *76*, 3762–3765.

(8) Karthaus, O.; Maruyama, N.; Cieren, X.; Shimomura, M.; Hasegawa, H.; Hashimoto, T. *Langmuir* **2000**, *16*, 6071–6076.

(9) Nishikawa, T.; Ookura, R.; Nishida, J.; Arai, K.; Hayashi, J.; Kurono, N.; Sawadaishi, T.; Hara, M.; Shimomura, M. *Langmuir* **2002**, *18*, 5734–5740.

(10) Nishikawa, T.; Nonomura, M.; Arai, K.; Hayashi, J.; Sawadaishi, T.; Nishiura, Y.; Hara, M.; Shimomura, M. *Langmuir* **2003**, *19*, 6193–6201.

(11) Yabu, H.; Tanaka, M.; Ijiri, K.; Shimomura, M. *Langmuir* **2003**, *19*, 6297–6300.

(12) Park, M. S.; Kim, J. K. *Langmuir* **2004**, *20*, 5347–5352.

(13) Peng, J.; Han, Y.; Yang, Y.; Li, B. *Polymer* **2004**, *45*, 447–452.

(14) Saunders, A. E.; Shah, P. S.; Sigman, M. B., Jr.; Hanrath, T.; Hwang, H. S.; Lim, K. T.; Johnston, K. P.; Korgel, B. A. *Nano Lett.* **2004**, *4*, 1943–1948.

(15) Shah, P. S.; Sigman, M. B., Jr.; Stowell, C. A.; Lim, K. T.; Johnston, K. P.; Korgel, B. A. *Adv. Mater.* **2003**, *15*, 971–974.

(16) Böker, A.; Lin, Y.; Chiapperini, K.; Horowitz, R.; Thompson, M.; Carreon, V.; Xu, T.; Abetz, C.; Skaff, H.; Dinsmore, A. D.; Emrick, T.; Russell T. P. *Nat. Mater.* **2004**, *3*, 302–306.

(17) Matsushita, S. I.; Kurono, N.; Sawadaishi, T.; Shimomura, M. *Synth. Met.* **2004**, *147*, 237–240.

(18) Haupt, M.; Miller, S.; Sauer, R.; Thonke, K.; Mourran, A.; Moeller, M. *J. Appl. Phys.* **2004**, *96*, 3065–3069.

(19) Yabu, H.; Shimomura, M. *Langmuir* **2005**, *21*, 1709–1711.

(20) Yabu, H.; Takebayashi, M.; Tanaka, M.; Shimomura, M. *Langmuir* **2005**, *21*, 3235–3237.

(21) Erdogan, B.; Song, L.; Wilson, J. N.; Park, J. O.; Srinivasarao, M.; Bunz, U. H. F. *J. Am. Chem. Soc.* **2004**, *126*, 3678–3679.

(22) Many commercial products related to NIR laser optics are available; see, for instance, <http://www.lasercomponents.de/www/index.html>.

(23) Wang, Y.; Cheng, X.; Lin, Z.; Zhang, C.; Xiao, H.; Zhang, F.; Zou, S. *Mater. Lett.* **2004**, *58*, 2261–2265.

(24) Macleod, H. A. *Thin-Film Optical Filters*; Hilger: Bristol, U.K., 1986; Chapter 3.

$$n_1 d_1 = n_2 d_2 = \lambda_0 / 4 \quad (1)$$

where n_i and d_i are the refractive index and thickness of individual layer i . Zero reflectance at a wavelength is obtained for the following relationship:²⁴

$$\frac{n_1^2 n_s}{n_2^2} = n_o \quad (2)$$

where n_s and n_o are the refractive indices of the substrate and air, respectively. To obtain the broad-band AR coating, films should have a gradual increase of n from the top to the substrate.^{25–30} A porous film also exhibits this kind of AR when it has two distinct asymmetric porous structures: top and bottom layers having higher and lower porosities, respectively. We found that a cellulose acetate butyrate (CAB) film prepared by spin-coating from the water-miscible solvent tetrahydrofuran (THF) under a humid environment exhibited the above-mentioned asymmetric porous structure. When the film thickness was carefully controlled, the porous film coated on a glass substrate showed low reflectance (below 1%) at broad-band NIR wavelengths.

2. Experimental Section

CAB was purchased from Acros Co., and the molecular characteristics are given in ref 12. Various solutions of CAB in chloroform, benzene, and THF were prepared and spin-coated on 2.5 cm × 2.5 cm glass. A glass slide was purchased from Corning Glass Works (Corning brand, plain (product no. 2947)), which was soda lime glass with a refractive index of 1.52. To measure reflectance, one side of the glass was spin-coated and the other side was sealed by black tape to eliminate backside reflection. The reflectance of the sample was measured with a UV–vis–NIR spectrophotometer (Cary 5000, Varian Co.) and a diffuse reflectance accessory (Internal DRA-2500, Varian Co.). The humidity during spin-coating was controlled by pouring 30 cm³ of hot water (85 °C) into the cylindrical chamber (25 cm in diameter and 10 cm in height) enclosing the spinning chuck on which the substrate was placed. Within 1 min, the relative humidity (RH) and temperature in the cylindrical chamber increased to 95% and 32 °C, respectively. The morphologies of the spin-coated films were investigated by field emission scanning electron microscopy (FE-SEM; Hitachi S-4200).

3. Results and Discussion

Figure 1 shows top and cross-sectional SEM images of a CAB film spin-coated from a 0.05 g/cm³ solution in THF at 7000 rpm under a humid environment (RH = 95%). The film surfaces were covered with pores generated from traces of condensed water droplets although perfectly hexagonal order of the pores was not observed. This is because each condensed water droplet does not have enough time to interact with other droplets due to the fast solidification of the solution during spin-coating, which prevents droplets from packing in an ordered lattice.¹² We found that porous films were prepared over a large area (several square centimeters). The average diameter and area fraction of the pores on the top surface were calculated to be 227 nm and 43.6%, respectively, from the

image analysis of the SEM image. From the cross-sectional image given in Figure 1c, the film shows two distinct porous structures. The top layer contains pores with relatively uniform size and close packing. The bottom (inner) layer has less porosity than the top layer. The total film thickness (d) obtained from the SEM image in Figure 1c was ~450 nm, which is consistent with that measured (~441 nm) by a height profile between the film surface and the substrate in an AFM image after the film was scratched by a razor. The depth of pores in the top layer was also determined to be 204 nm from the AFM height profile and height image as shown in the inset of Figure 1d. This value is close to that observed in the SEM image of Figure 1c.

It is noted that porous films prepared by a breath figure from the drop and evaporation method might have a multilayer porous morphology.^{5,12} Water droplets on the top surface can sink into the solution, and newly formed water droplets cover the surface of the solution. Repeated water condensation forms a 3-dimensional porous structure after complete drying of the solvent and water.⁵ On the other hand, consecutive inlet and sinking of water droplets into the polymer solution might be limited for the spin-coating under a humid environment method, because the solution is rapidly solidified during spin-coating. In this situation, after complete evaporation of water, porous films exhibit an asymmetric morphology: the top layer of the film has a higher pore fraction, while the bottom layer contains a smaller pore volume due to an insufficient number of water droplets.

The porous CAB film prepared in this study looked milky white, resulting from the scattering of visible light since the average pore diameter and d were 227 and ~450 nm, respectively. However, this film did not show a scattering at NIR wavelengths, where the glass and CAB did not have any absorption. Figure 2 shows that the reflectance of glass spin-coated on one side from a CAB solution (0.05 g/cm³) in THF at 7000 rpm under 95% RH was less than 1% at NIR wavelengths between 900 and 2200 nm. Two minima in the reflectance were observed at 958 nm (0.78%) and 1741 nm (0.77%). On the basis of the results given in Figure 2, we consider that the CAB film prepared by spin-coating under a humid environment could be used as a broad-band antireflection film at NIR wavelengths.

Low reflectance at broad wavelengths and multiple minima were not expected for an AR coating consisting of only a single layer with a uniform reflective index (n) throughout the entire film thickness. From Figure 1, we characterized the porous CAB film prepared in this study by using the two-layer model with the aid of the characteristic matrix theory:²⁴ the top layer with a thickness of 235 nm with $n = 1.290$ and the bottom layer with a thickness of 213 nm with $n = 1.445$. Since $n_1 d_1 \cong n_2 d_2$, this film satisfies the quarter wavelength thickness given in eq 1. The measured reflectance (symbol) is in good agreement with the calculated reflectance (line), as shown in Figure 2. The calculated total thickness from the theory is also consistent with that observed in the SEM image. Also, the effective n of the porous CAB film (n_e) in the top layer is calculated from $n_e^2 = n_o^2(1 - \phi) + \phi$, in which n_o and ϕ are the n (1.49) of a pure CAB film and porosity, respectively.^{30,31} Using $\phi = 0.436$ obtained from the top view of the SEM image (Figure 1a), the calculated n_e was 1.299, very similar to that (1.290) predicted by the theory. It is mentioned that, for a given $n_2 = 1.445$ (the characterized value for the bottom layer of the above film),

(25) Kintaka, K.; Nishii, J.; Mizutani, A.; Kikuta, H.; Nakano, H. *Opt. Lett.* **2001**, *26*, 1642–1644.

(26) Minot, M. J. *J. Opt. Soc. Am.* **1976**, *66*, 515–519.

(27) Koo, H. Y.; Yi, D. K.; Yoo, S. J.; Kim, D. *Adv. Mater.* **2004**, *16*, 274–277.

(28) Walheim, S.; Schäffer, E.; Mlynek, J.; Steiner, U. *Science* **1999**, *283*, 520–522.

(29) Hiller, J.; Mendelsohn, J. D.; Rubner, M. F. *Nat. Mater.* **2002**, *1*, 59–63.

(30) Yoldas, B. E. *Appl. Opt.* **1980**, *19*, 1425–1429.

(31) Park, M. S.; Lee Y.; Kim, J. K. *Chem. Mater.* **2005**, *17*, 3944–3950.

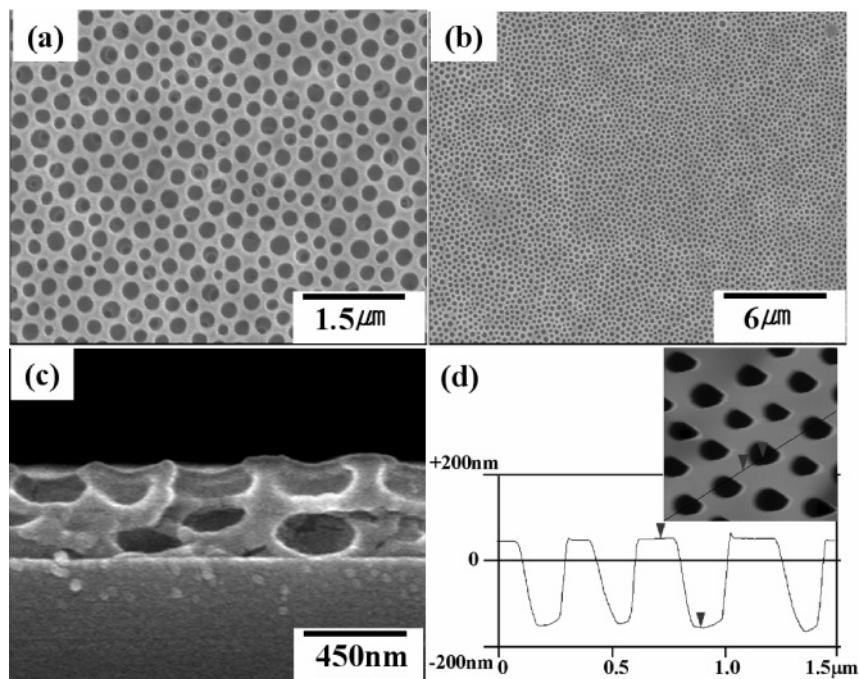


Figure 1. SEM images of top views at a high (a) and a low (b) magnification and (c) cross-sectional view of a spin-coated CAB film from a 0.05 g/cm^3 solution in THF at 7000 rpm under an RH of 95%. (d) AFM height profile. The inset is the height AFM image ($1.3 \mu\text{m} \times 1.3 \mu\text{m}$).

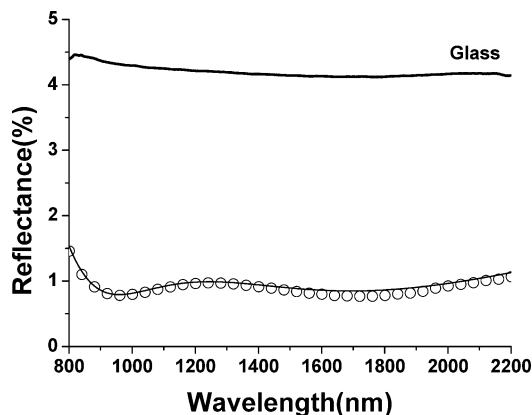


Figure 2. Reflectance of glass spin-coated with a CAB film on one side from a 0.05 g/cm^3 solution in THF at 7000 rpm under an RH of 95%. The symbols and solid line represent the measured and calculated reflectances from the characteristics matrix theory, respectively. The reflectance of bare glass was added for reference.

the ideal value of n_1 estimated by eq 2 is 1.172, which is smaller than the characterized n_1 (1.290) for this film. Thus, as the porosity of the top layer increases further, a better broad-band AR effect could be achieved. However, the average reflectance (0.88%) at 900–2200 nm was shown to be lower than 1%, which can be practically employed for AR coating.

We also studied the effect of d on the porous morphology of the CAB film and reflectance in the NIR region by changing the CAB solution concentration in THF. Figure 3 shows the top and cross-sectional SEM images of a spin-coated CAB film from a 0.08 g/cm^3 solution in THF at 7000 rpm under a humid environment (RH = 95%). d of this porous film was 690 nm, measured from the cross-sectional SEM image, and one might be tempted to consider that this porous film exhibited two distinct porous layers. The top layer with $d_1 = 210 \text{ nm}$ contained pores with relatively uniform size, and the inner layer with $d_2 = 480 \text{ nm}$ had less porosity than the top layer. Although

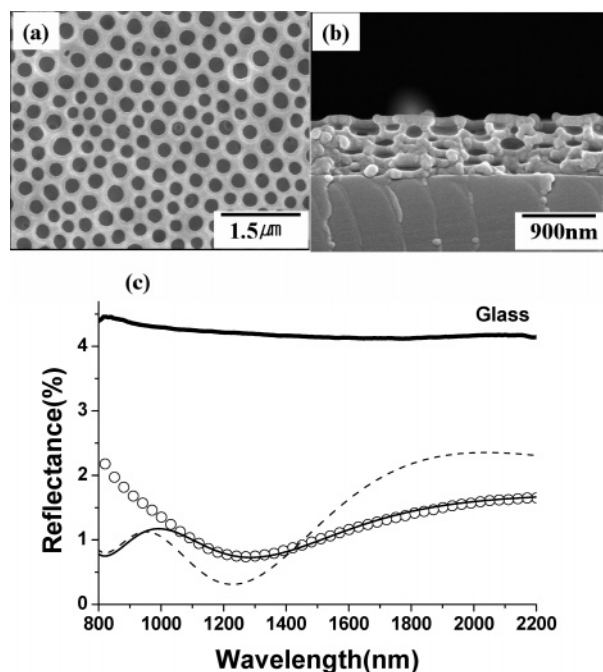


Figure 3. (a) Top and (b) cross-sectional SEM images of a spin-coated CAB film from a 0.08 g/cm^3 solution in THF at 7000 rpm under an RH of 95%. (c) Reflectance of glass spin-coated with CAB on one side from a 0.08 g/cm^3 solution in THF at 7000 rpm under an RH of 95%. The symbols represent the measured reflectances. Dashed and solid lines represent calculated reflectances by two-layer and three-layer porous structures from the characteristic matrix theory, respectively. The reflectance of bare glass was added for reference.

this film exhibited a minimum in reflectance of 0.74% at 1275 nm, it does not satisfy the quarter wavelength thickness for the two-layer structure given in eq 1. Namely, $n_1 d_1$ could not be the same (even similar to) as $n_2 d_2$, because $d_1 < d_2$ and $n_1 < n_2$. Thus, this film did not show an effective broad-band AR compared with the film given in Figure 2. We found that the fit by the two-layer model, which

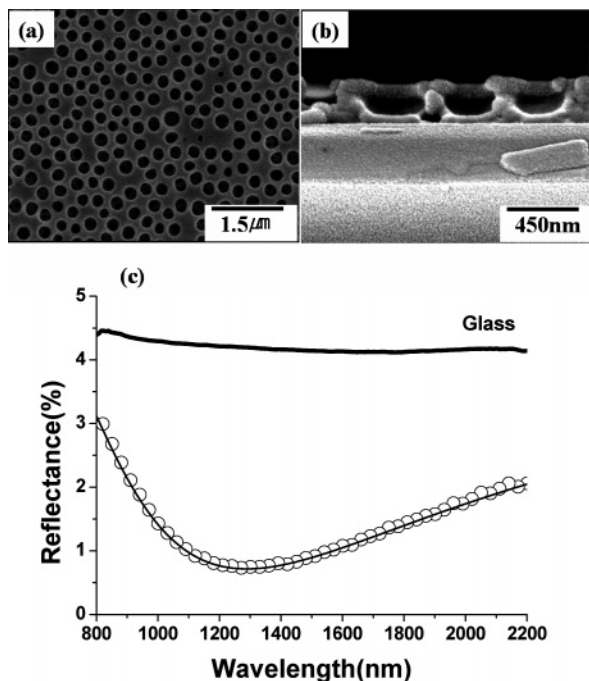


Figure 4. (a) Top and (b) cross-sectional SEM images of a spin-coated CAB film from a 0.03 g/cm^3 solution in THF at 7000 rpm under an RH of 95%. (c) Reflectance of glass spin-coated with CAB on one side from a 0.03 g/cm^3 solution in THF at 7000 rpm under an RH of 95%. The symbols and solid line represent the measured and calculated reflectances from the characteristic matrix theory, respectively. The reflectance of bare glass was added for reference.

characterizes the film with $n_1 = 1.295$ and $d_1 = 210 \text{ nm}$ for the top layer and $n_2 = 1.445$ and $d_2 = 480 \text{ nm}$ for the inner layer, showed significant deviation from the measured reflectance (dashed line in Figure 3c). The failure of the two-layer model is because the pore population in the inner layer is not homogeneously distributed, as shown in the cross-sectional SEM image (Figure 3b). Rather, this film can be assumed to have a three-layer porous structure. When we used the characteristic matrix theory by using the three-layer porous structure, the film was characterized: $n_1 = 1.297$ and $d_1 = 210 \text{ nm}$ for the top layer, $n_2 = 1.430$ and $d_2 = 200 \text{ nm}$ for the middle layer, and $n_3 = 1.480$ and $d_3 = 280 \text{ nm}$ for the bottom layer. But these conditions do not satisfy the quarter wavelength thickness for the three-layer model. The predicted reflectances given by the solid line in Figure 3c are in good agreement with the observed ones, except at short wavelengths (800–1100 nm). The discrepancy at smaller wavelengths might be attributed to the fact that scattering (or diffuse reflectance) resulting from larger pores and film roughness is not negligible at shorter wavelengths, and the scattering increases with increasing film thickness. Since the scattering effect is not negligible in this film, the minimum in reflectance at 1275 nm in Figure 3 would not result from the interference effect itself. If the scattering is reduced by decreasing the pore sizes, broad-band AR coating with lower reflectance than that in Figure 3 could be achieved even for a thicker porous film. The reason that a three-layer porous structure was formed in this film might be an increased total film thickness which can accommodate more than three layers of water droplets. The detailed mechanism for the generation of multiple porous layers depending on the film thickness will be reported in a future paper.

Figure 4 shows the top and cross-sectional SEM images of a spin-coated CAB film from a 0.03 g/cm^3 solution in

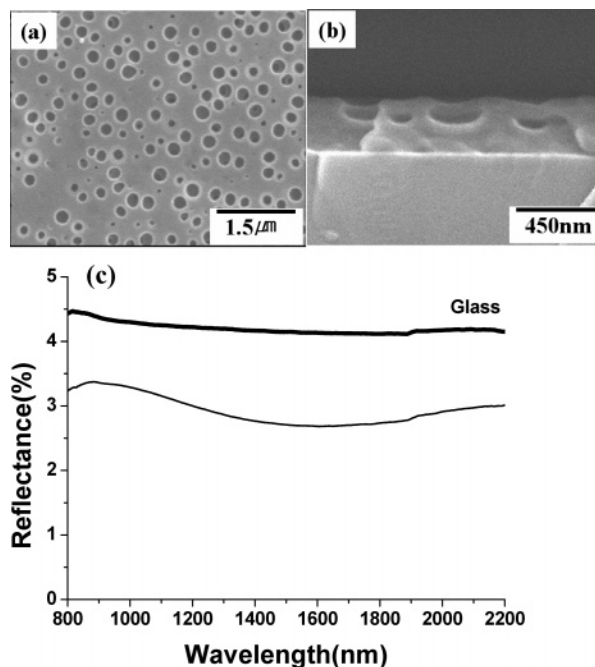


Figure 5. (a) Top and (b) cross-sectional SEM images of a spin-coated CAB film from a 0.05 g/cm^3 solution in chloroform at 7000 rpm under an RH of 95%. (c) Reflectance of glass spin-coated with a CAB film on one side from a 0.05 g/cm^3 solution in chloroform at 7000 rpm under an RH of 95%. The reflectance of bare glass was added for reference.

THF at 7000 rpm under a humid environment (RH = 95%). Interestingly, only a single porous layer, not a two-layer morphology, was observed, because d of this film ($\sim 240 \text{ nm}$) is similar to the diameter (227 nm) of the pores. This film does not exhibit a reflectance smaller than 1% at a wide range of wavelengths, even though a minimum in the reflectance (0.74%) was observed at 1274 nm. Analysis of the film by the characteristic matrix theory using a single-layer film gave a refractive index of 1.34 and a total film thickness of 238 nm. According to eq 1, the measured value of λ_0 (1274 nm) is in good agreement with the predicted one ($1286 \text{ nm} = 4 \times 1.34 \times 238 \text{ nm}$). The predicted reflectance on the basis of a single layer of porous structure is in good agreement with the measured one. When the CAB concentration in THF was lower than 0.03 g/cm^3 , a porous CAB film was not generated by a breath figure due to the very small thickness.

In this study, a breath figure was formed from a water-miscible solvent such as THF described in a previous paper,¹² although condensed water droplets could mix into the solution. This might be due to the fact that condensed water droplets could be embedded in the THF solution without mixing for short times either by Marangoni convection resulting from a temperature difference³² or by fast evaporation and the increase in viscosity prohibiting the coalescence of the water droplets.¹² It is interesting to find whether a water-immiscible solvent such as chloroform can generate a porous film prepared by spin-coating under humid conditions. Figure 5 gives the top and cross-sectional SEM images of a CAB film prepared by spin-coating from a 0.05 g/cm^3 solution in chloroform at 7000 rpm under an RH of 95%. Interestingly, the area fraction of the pores on the film surface was 12.2%, much lower than that (43.0%) of a film prepared from THF solution. This film did not exhibit an effective AR due to the low porosity (higher refractive index) of the top layer,

as shown in Figure 5c. The morphology of the porous CAB film prepared by spin-coating from a benzene solution was similar to that of a film prepared from a chloroform solution. These results suggest that condensed water droplets by a breath figure could be better embedded into a THF solution compared with water-immiscible solvent (chloroform and benzene) solutions during spin-coating. On the other hand, we previously showed that a well-ordered porous structure was generated for a CAB solution in chloroform from the drop and evaporation method and the hexagonal packing in the pores prepared from a water-immiscible solvent solution was better than that obtained with a THF solution.¹² The reason that spin-coating from the latter solution under a humid environment gives more pores at the top surface in the porous film compared with that from the former solution is as follows. During spin-coating, the total amount of the solvent to cause evaporative cooling would be considerably smaller compared to that in the drop and evaporation method, because a large amount of the solution dropped on the substrate was removed at the beginning of spin-coating. Also, the polymer solution was fast solidified during spin-coating. In this situation, nucleation of condensing water onto the solution at the early stage of spin-coating would be critical. From classical nucleation theory for the formation of a new phase, the free energy change (ΔG) during condensation is given by³³

$$\Delta G = -\frac{4}{3}\pi r^3 \frac{1}{\bar{V}} RT \ln \frac{P}{P_0} + 4\pi r^2 \gamma \quad (3)$$

where \bar{V} , r , and γ are the molar volume, radius, and surface tension of the droplets and P and P_0 are the vapor pressures in the vapor phase and droplet, respectively. For condensation onto the liquid (namely, a breath figure on the fluid),^{34,35} all of the water droplets cannot be covered by the solution. In this case, eq 3 becomes

$$\Delta G = -\frac{4}{3}\pi r^3 \frac{1}{\bar{V}} RT \ln \frac{P}{P_0} + \gamma_w A_1 + \gamma_{w/s} A_2 - \gamma_s B \quad (4)$$

where A_1 and A_2 are the contact areas of the droplets with air and with the solution and B is the disappearing area of the solution covered by the water droplets. γ_w and γ_s are the surface tensions of water and the solution,

(33) Adamson, A. W. *Physical Chemistry of Surfaces*, 4th ed.; Wiley-Interscience: New York, 1982; Chapter 9.

(34) Knober, C. M.; Beysens, D. *Europhys. Lett.* **1988**, *6*, 707–712.

(35) Bolognesi, A.; Mercogliano, C.; Yunus, S.; Civardi, M.; Comoretto, D.; Turturro, A. *Langmuir* **2005**, *21*, 3480–3485.

respectively, and $\gamma_{w/s}$ is the interfacial tension between water and the solution. For the assumption of the same droplet size, A_1 , A_2 , and B for THF and chloroform, ΔG for the THF solution is lower than that for the chloroform solution by $\gamma_{w/\text{chloroform}}$. This is because γ_s (26.4 ergs/cm²) and ΔH_{vap} (0.36 kJ/cm³) of THF are similar to those (27.5 ergs/cm² and 0.35 kJ/cm³) of chloroform and $\gamma_{w/\text{THF}}$ would be negligibly small due to the miscibility. Thus, the maximum value of ΔG (ΔG_{max}) to overcome the energy barrier to form nuclei on the THF solution is less than that to overcome the energy barrier to form nuclei on the chloroform solution. This suggests that the nucleation rate (I) expressed by $\exp(-\Delta G_{\text{max}}/RT)$ for the former is larger than that of the latter. According to this simple calculation, water droplet condensation onto the THF solution would be much favored over that onto the chloroform solution at the beginning of spin-coating.

We show that a porous film prepared by spin-coating of a polymer solution in a water-miscible solvent under humid conditions can be employed for an AR film. However, the stability of this film in different environments should be carefully checked for practical applications. We consider that good adhesion and wear and scratch resistance would be achieved without sacrificing the AR effect, when films with functional groups capable of reacting with the substrate are coated onto the substrate or the film is cross-linked.

4. Conclusion

In this study, we extended spin-coating under a humid environment to generate a broad-band antireflection effect in the NIR region. When d was controlled to be 400–600 nm, a two-layer porous structure with the top layer with higher porosity and the bottom layer with smaller porosity was successfully generated. This two-layer porous film coated on glass exhibited low reflectance of less than 1% in the NIR region. Since the porous structure was very uniform over a large area, the film could be easily employed for broad-band antireflection coating at NIR wavelengths. We found that a broad-band AR effect at NIR wavelengths was better achieved from spin-coating of a water-miscible solvent than a water-immiscible solvent. The difference in generating pores by a breath figure from a water-miscible solvent and a water-immiscible solvent was mainly due to the different nucleation rates for condensed droplets on the solution.

Acknowledgment. This work was supported by the Creative Research Initiative Program.

LA051273G